Acta Polytechnica CTU Proceedings **55**:8–15, 2025
https://doi.org/10.14311/APP.2025.55.0008

Published by the Czech Technical University in Prague

CORROSION BEHAVIOUR OF AISI 348 STAINLESS STEEL IN SIMULATED WWER ENVIRONMENT AND DURING LOCA CONDITIONS

Václav Bouček[a,b,*], Jakub Krejčí[b], Martin Cesnek[a], Jitka Kabátová[b], Martin Ševeček[a]

[a] *Czech Technical University in Prague, Faculty of Nuclear Sciences and Physical Engineering, Břehová 7, 115 19 Prague 1, Czech Republic*

[b] *UJP Praha a.s., Nad Kamínkou 1345, 156 00 Prague, Czech Republic*

[*] corresponding author: boucevac@fjfi.cvut.com

Abstract. This study investigates the corrosion and high-temperature oxidation behaviour of AISI 348 stainless steel under normal and extreme conditions for potential nuclear applications.

Plate specimens were exposed to simulated WWER primary water conditions in an autoclave at 360 °C for extended duration, reaching up to 1659 days. In addition to long-term exposure testing, short-term high-temperature oxidation experiments were performed at temperatures up to 1 400 °C to evaluate oxide scale formation, spallation behaviour, and structural integrity. Characterization techniques included Mössbauer spectroscopy for oxide phase identification, microhardness measurements, and optical microscopy for grain size evaluation. Mechanical testing, including ductility assessment and microhardness measurements, was conducted after high-temperature exposure to evaluate the material's ability to retain mechanical integrity under accidental conditions.

Keywords: AISI 348, stainless steel, corrosion, LOCA conditions, WWER.

1. Introduction

Austenitic stainless steels, particularly stabilized grades like AISI 348 or AISI 321, are widely employed in nuclear reactor systems due to their excellent high-temperature strength and corrosion resistance. In pressurized water reactors such as the WWER (Water-Water Energetic Reactor), structural materials are exposed to aggressive conditions including high-temperature water, dissolved boric acid, lithium or potassium hydroxide, oxygen, hydrogen, and intense neutron irradiation. These factors can lead to complex corrosion phenomena such as inter-granular attack, stress corrosion cracking, and irradiation-assisted corrosion.

In recent years, stainless steels have also gained attention as potential candidates for Accident Tolerant Fuel (ATF) cladding due to their high-temperature oxidation resistance and superior mechanical performance under severe accident conditions. Their robustness and ability to retain structural integrity during transient high-temperature events make them promising alternatives to zirconium-based alloys. This study investigates the corrosion behaviour under simulated WWER primary circuit conditions and high-temperature oxidation resistance of AISI 348 stainless steel, with a focus on understanding material degradation mechanisms and assessing the suitability of this alloy for long-term service in nuclear environments.

2. Materials and methods

These specimens were tested as part of the IAEA CRP ACTOF project, in which the results of a long-term corrosion experiment lasting up to 164 days were previously presented [1]. In this article, results from an extended exposure period of up to 1659 days are reported. Moreover, extended results of high-temperature oxidation are shown. The AISI 348 specimens were provided by USP, Brazil. The chemical composition provided by the supplier is shown in Table 1.

2.1. Long-term corrosion

Specimens for long-term corrosion had dimensions of $20 \times 20 \times 5$ mm and included a 2 mm hole for suspension on a holder and were tested in a simulated WWER environment consisting of demineralized and deaerated water containing 1050 ppm boron (as H_3BO_3), 16 ppm potassium (as KOH), and 1 ppm lithium (as LiOH). The corrosion experiment was conducted in a static autoclave with an internal volume of 4.4 dm^3 at a temperature of 360 °C and a corresponding pressure of 18.6 MPa. Testing intervals typically lasted 21 days. The temperature was set higher than that of WWER-1000 outlet water to accelerate corrosion, to simulate potential elevated cladding temperatures, and to allow comparison with results from other laboratories conducting tests at the same temperature.

After each interval, the autoclave was shut down and opened. The specimens were washed with distilled water, dried, and weighed using a laboratory balance

Element	C	Mn	P	S	Si	Cr	Ni	Nb	N	Co	Ta	B	Fe
Wt. %	0.055	1.70	0.017	0.003	0.41	17.5	11.0	0.85	0.018	0.021	<0.005	0.0008	Bal.

TABLE 1. Chemical composition of AISI 348 stainless steel.

with a precision of 10^{-5} g. They were then returned to the autoclave, and the next testing period commenced.

2.2. HIGH-TEMPERATURE OXIDATION

High-temperature oxidation tests were conducted on tubular specimens in an electric resistance furnace in argon-steam atmosphere (1 100, 1 200, 1 300, and 1 400 °C) for predetermined time intervals and then quenched in a water-ice mixture. These conditions were defined based on considerations for the standard DBA fuel safety criteria such as 17 % ECR limit and cladding embrittlement calculated using the Cathcart-Pawel correlation [2]. Additionally, previous experience with testing of ATF cladding materials was used to define the test duration [3].

Subsequently, the specimens were sectioned and subjected to ring compression testing, microhardness measurements, metallographic analysis, and hydrogen content measurement.

Ring compression tests were performed on an INSTRON 1185 R5800 at 135 °C (displacement rate 1 mm min^{-1}), Vickers microhardness (HVM 0.1) was measured using Buehler MICROMET 5114. Microstructure of the specimens was analyzed using a light optical microscope Nikon EPIPHOT 300 and scanning electron microscope JEOL JSM-5510LV equipped with EDS detector. Bulk hydrogen content was measured using the Bruker G8 Galileo Analyzer.

2.3. MÖSSBAUER SPECTROSCOPY (CEMS)

Surface of samples after corrosion exposure in the autoclave for 63 and 1659 days was analyzed using Conversion Electron Mössbauer Spectroscopy (CEMS). Sample after 63 days of exposure is displayed in Figure 1.

CEMS spectrum was recorded at room temperature (RT) using a constant acceleration spectrometer with a ^{57}Co(Rh) source. The resulting isomer shifts are quoted relative to the MS spectrum of a bcc-Fe foil recorded at RT. All the MS spectral parameters such as isomer shift (IS), quadrupole splitting (QS), hyperfine magnetic field (B_{hf}) and area (A) of spectral components including relative intensities of the lines in sextets were refined by the CONFIT curve-fitting software [4]. Mössbauer spectroscopy is a technique that uses the ^{57}Fe nucleus as a probe and is extremely sensitive to changes in its local environment. In conversion electron Mössbauer spectroscopy (CEMS), secondary electrons generated by resonant absorption are detected instead of γ-photons, making the method highly surface-sensitive, typically probing a depth of up to approximately 200 nm, depending on the matrix composition.

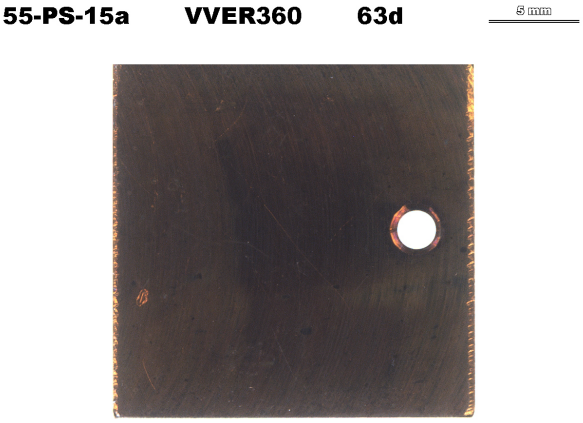

FIGURE 1. Sample of AISI 348 steel after exposure in simulated WWER conditions at 360 °C for 63 days.

3. RESULTS

3.1. LONG-TERM CORROSION

The results of the weight gain measurements during long-term exposure are presented in Figure 2 (left). The weight gain of AISI 348 specimens ranged from approximately 1 to 2 mg dm^{-2} over the entire testing period. This relatively low mass increase indicates stable oxide layer formation and limited corrosion progression, even after prolonged exposure under simulated WWER primary circuit conditions. A distinct increase in WG between 816 and 841 days of exposure is noticeable in the graph, which may be attributed to the presence of an adhered impurity. Following this increase, the WG gradually decreased as the impurity dissolved. However, all WG values are close to the resolution limit of the balance, which contributes to the observed data scatter.

For context, the graph also includes previously obtained data for Zircaloy-4 tested in the same environment, Figure 2 (right), using historical results from UJP. The comparison clearly illustrates that AISI 348 exhibits significantly lower weight gain compared to Zircaloy-4. This suggests superior corrosion resistance, which is a critical factor in evaluating candidate materials for Accident Tolerant Fuel (ATF) cladding.

These findings further support the viability of austenitic stainless steels as long-term structural materials in nuclear environments and reinforce their potential role as an alternative to zirconium-based alloys in ATF applications.

Figure 3 shows images of specimen SS-PS-13 after 21 days and after 1659 days of exposure in the simulated WWER environment. Both images were taken from the same side of the specimen. As evident

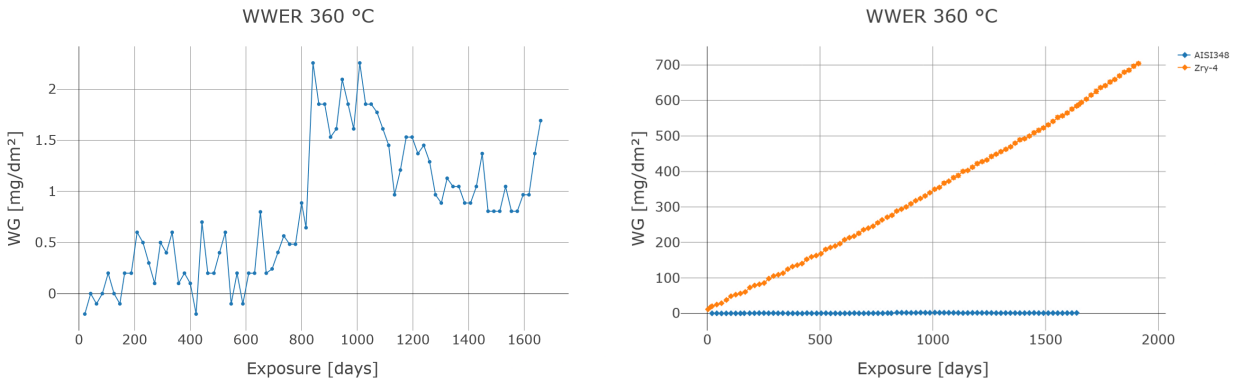

Figure 2. Weight gain after exposure in autoclave in simulated WWER environment. Left – AISI 348 specimen, Right – Comparison with Zry-4 specimen.

Figure 3. Pictures of the same specimen from the same side after 21 days (top) and 1659 days (bottom) of exposure in the WWER environment.

from the comparison, a protective oxide layer formed during the initial exposure period (21 days) and its appearance remains almost unchanged throughout the entire testing duration. This suggests the oxide layer is stable and does not undergo significant changes over time. The images were taken at least five years apart under different lighting conditions. Although the specimen after 1659 days appears darker than the 21-day sample, this does not necessarily indicate more extensive oxidation. Color differences depend on lighting, operator, and specimen illumination, so oxidation should be assessed primarily from weight gain.

3.1.1. Mössbauer spectroscopy

The CEMS spectrum has been recorded at room temperature for specimens after 63 and 1659 days of exposure in simulated WWER environment.

The spectrum after 63 days is shown in Figure 4 (left). The dominant contribution to the spectrum arises from a broad sextet that corresponds to the martensitic α'-Fe phase. Due to the presence of various minor alloying elements in the local environment of ^{57}Fe nuclei, the hyperfine magnetic field is not discrete but rather distributed. Therefore, the martensitic component was modeled using two distributed sextets. The mean hyperfine magnetic field of this component is 31.8 ± 0.5 T, and the mean isomer shift is -0.03 ± 0.02 mm s^{-1}. The corresponding hyperfine field distribution is shown in Figure 4 (right), which illustrates the inhomogeneous local atomic environment in the martensitic phase.

A central singlet, also visible in the spectrum, is attributed to the paramagnetic γ-Fe phase, characterized by an isomer shift of -0.13 ± 0.02 mm s^{-1}. In addition, a weak doublet with a relative spectral area of 2.8 % was identified. Its hyperfine parameters, IS $= 0.34 \pm 0.02$ mm s^{-1} and QS $= 0.66 \pm 0.04$ mm s^{-1}, closely resemble those reported for $FeCr_2O_4$ by Waanders et al. [5].

No other iron oxides were observed. Notably, Fe-based oxides such as magnetite or hematite typically exhibit much higher hyperfine magnetic fields (around 50 T), and would therefore produce sextets located near the velocity regions indicated by red arrows in Figure 4 (left). While no distinct sextet pattern appears in these regions, a slightly elevated baseline is noticeable, potentially indicating the initial stages of Fe oxide formation.

A follow-up CEMS measurement was performed after 1659 days of exposure at 360 °C in simulated

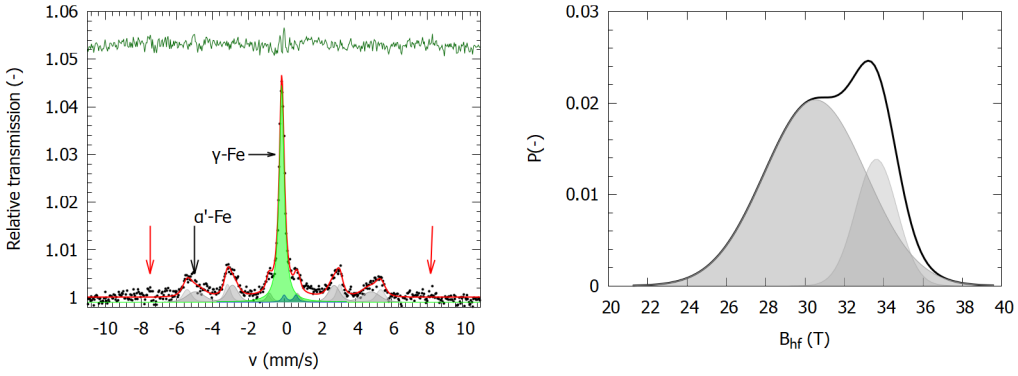

FIGURE 4. CEMS spectrum of the sample annealed at 360 °C for 63 days. The spectrum shows a distributed sextet corresponding to the α'-Fe martensitic phase (gray), a singlet corresponding to γ-Fe (green), and a minor doublet likely due to $FeCr_2O_4$. Red arrows indicate expected regions for sextets of Fe-based oxides with $B_{hf} \approx 50$ T. Hyperfine magnetic field distribution of the α'-Fe martensitic phase.

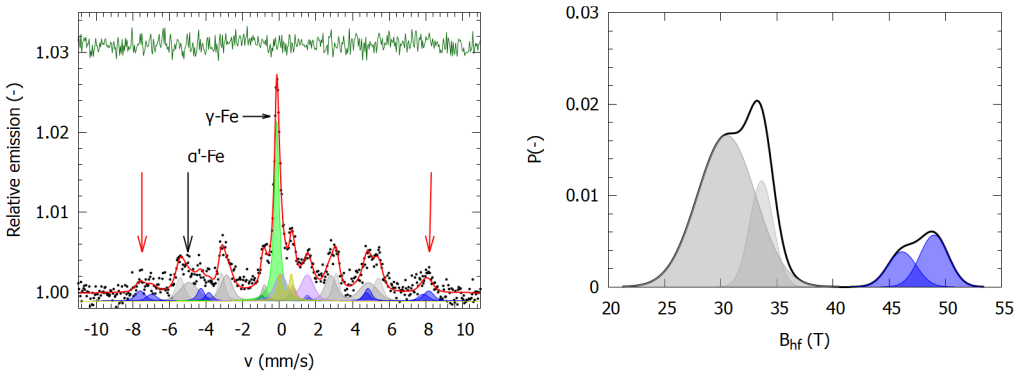

FIGURE 5. CEMS spectrum of the sample after 1659 days of annealing at 360 °C (left). Hyperfine field distribution showing contributions from both martensitic and oxide phases (right).

WWER environment. The corresponding spectrum and hyperfine magnetic field distribution are shown in Figure 5 (left). In addition to the retained martensitic α'-Fe and γ-Fe phases, sextet features (displayed in blue) emerged in the high-field region fitted with hyperfine parameters: IS $= 0.28 \pm 0.02\,\mathrm{mm\,s^{-1}}$, B_{hf} $= 49.0 \pm 0.5$ T and IS $= 0.45 \pm 0.02\,\mathrm{mm\,s^{-1}}$, B_{hf} $= 46.2 \pm 0.5$ T, both having negligible quadrupole shift. Such components might suggest formation of non-stoichiometric magnetite [6].

In addition to the previously observed $FeCr_2O_4$-like doublet, a new paramagnetic doublet (displayed in purple) with IS $= 0.79 \pm 0.02\,\mathrm{mm\,s^{-1}}$ and QS $= 1.48 \pm 0.04\,\mathrm{mm\,s^{-1}}$ was detected. This component might be associated with Fe^{2+} in a mixed oxide spinel-type structure [7]. The relative spectral areas of the oxide-related components were 0.15 ± 0.03 for non-stoichiometric magnetite, 0.06 ± 0.01 for Fe^{3+} in mixed oxides, and 0.12 ± 0.01 for Fe^{2+} in mixed oxides.

3.2. High-temperature oxidation

Four tubular specimens were tested under simulated Loss-of-Coolant Accident (LOCA) conditions in a steam–argon environment at four different temperatures: 1 100 °C, 1 200 °C, 1 300 °C, and 1 400 °C. Exposure times were adjusted accordingly to 60, 30, 5, and 2 minutes, respectively. Following exposure, all specimens were quenched in a water–ice mixture. Strong oxide spallation was observed on all samples, as illustrated in Figure 6. After testing, weight gain (WG) and remaining wall thickness were measured; results are summarized in Table 2. The highest weight gain was recorded after exposure at 1 400 °C – almost three times greater than the values obtained from significantly longer exposures at 1 100 and 1 200 °C. A decrease in remaining wall thickness was observed with increasing temperature; for all four specimens, the final wall thickness ranged from 40 % to 60 % of the original.

High-temperature exposure affected not only the oxide layer but also the microstructure of bulk material. Microstructural evolution is documented in Figure 6 (right). The average grain size of the as-received material was in the range of ASTM grain size number 8–9 (per ASTM E112) according to supplier. This grain size corresponds to ČSN EN ISO 643 [8] grain size number G 8–9. Grain size after high-temperature exposure was measured according to ČSN EN ISO 643 standard. After exposure at 1 100 °C, a slight grain refinement was observed (grain size number G 10.5). However, at higher temperatures, significant grain

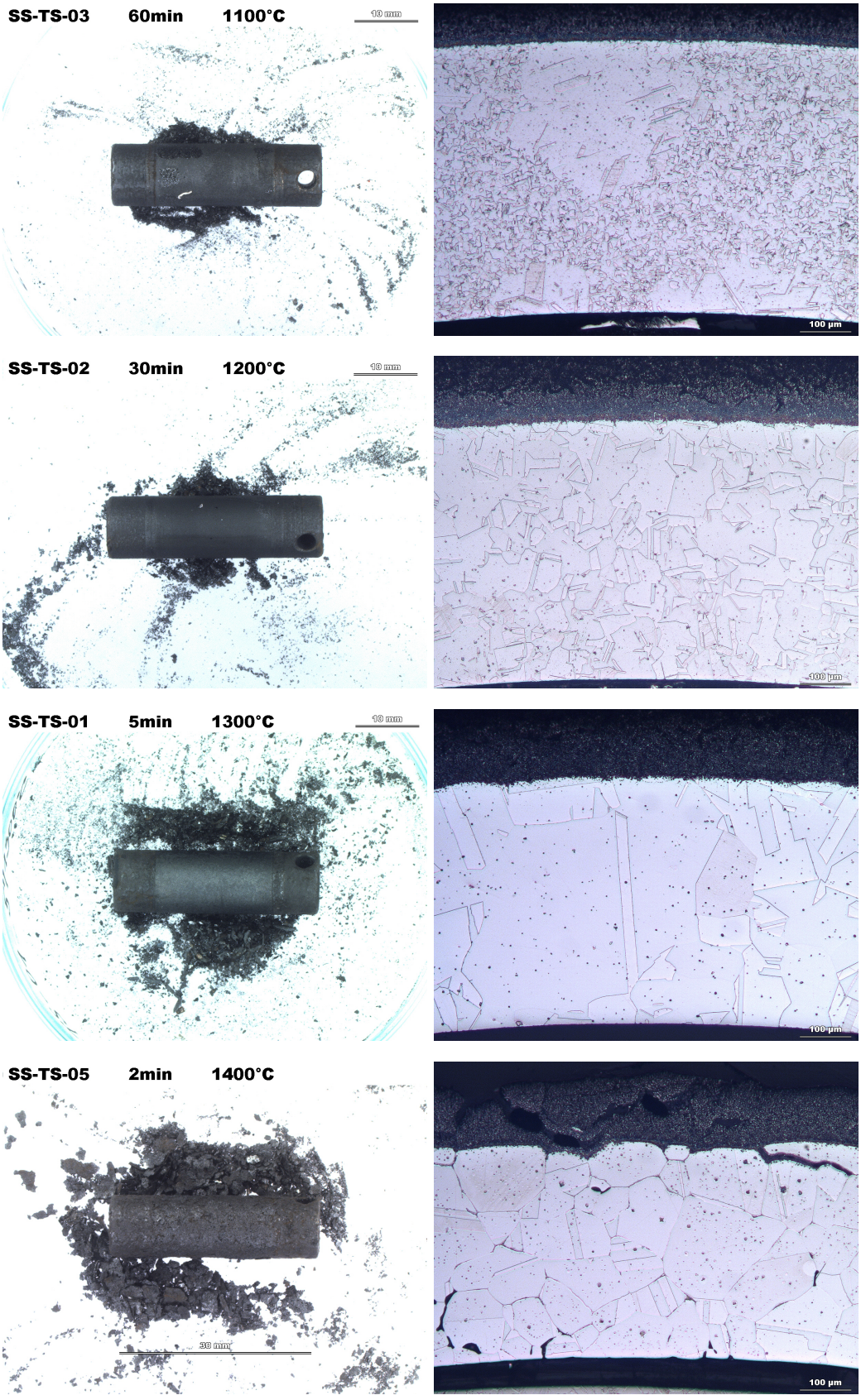

Figure 6. Pictures of tubular specimens after high-temperature tests (left) and corresponding microstructure (right). Top down 1 100, 1 200, 1 300, and 1 400 °C.

Exposure [°C/min]	WG [mg dm^{-2}]	Wall thickness [µm]	HVM 0.1	H [ppm]	RCT [%]	Grain size (ISO 643)
As-received	–	928	150–200	–	–	8–9
1 100/60	737	538	162	9.2	11.49/10.60	10.5*
1 200/30	619	516	145	8.3	17.06/18.24	6
1 300/5	1 122	485	150	5.9	17.04/18.12	3
1 400/2	2 174	418	160	12.1	18.55/19.59	4

* excluding coarse areas

TABLE 2. Results of high-temperature oxidation experiments. Two rings were used for ring compression test, therefore two values are presented.

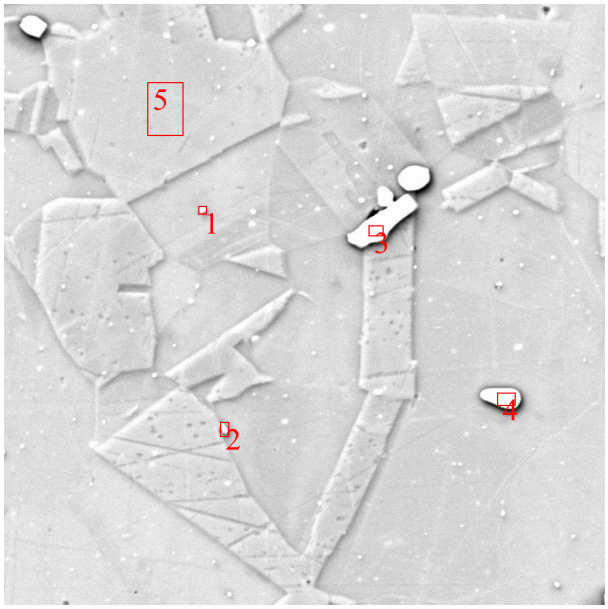

FIGURE 7. Areas of SEM-EDS analysis of specimen after high-temperature exposure at 1 100 °C.

Area	C	Cr	Mn	Fe	Ni	Nb
1	4.22	14.65	1.06	51.35	7.84	20.88
2	5.22	15.27	1.42	54.54	8.77	14.78
3	5.46	1.09	0.17	2.66	0.29	90.32
4	8.93	2.10	0.26	5.02	0.85	82.84
5	0.00	17.30	1.45	69.78	10.75	0.71

TABLE 3. Results of SEM-EDS analysis of specimen after high-temperature exposure at 1 100 °C.

coarsening occurred. After exposure at 1 300 °C and 1 400 °C, grain sizes were measured in the range of G 3–4. Additionally, localized areas with coarse grains were observed even after exposure at 1 100 °C (Figure 6, top right), occurring on both inner and outer surfaces of the specimen wall. These areas were excluded from average grain size measurements. Across all images, small particles – identified by EDS as niobium-rich carbides – are visible within the grains (Figure 7 and Table 3). In the bottom image of Figure 6, some grain boundaries appear to show signs of intergranular corrosion (in detail Figure 8).

Mechanical properties were evaluated using the ring

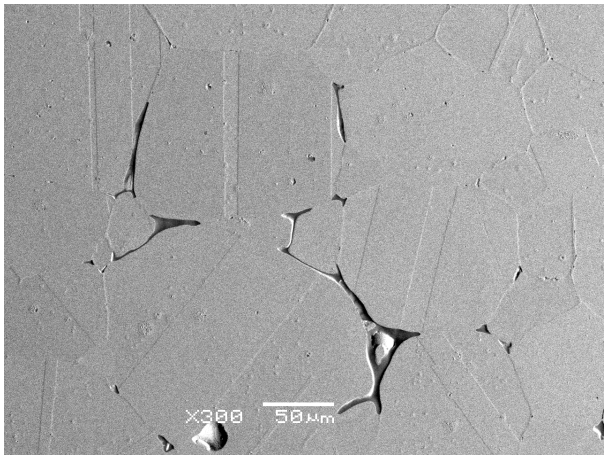

FIGURE 8. Specimen after 1 400 °C/2 minutes exposure, secondary electrons, topographic mode.

compression test (RCT). Two ring samples were cut from each tubular specimen and tested at 135 °C. Most samples exhibited elongation of approximately 18 %, except for the specimen exposed at 1 100 °C, which showed reduced ductility with elongation around 11 %.

Microhardness of the as-received material ranged from 150 to 200 according to supplier. After all exposures, hardness values remained near the lower end of this interval (measured according to [9] standard). Hydrogen content after high-temperature oxidation remained low, with a maximum measured value of 12.1 ppm after the 1 400 °C/2-minute test.

The low hydrogen uptake suggests that most of the hydrogen produced during oxidation escaped to the environment. Released hydrogen has been evaluated in the IAEA report [1], in the section contributed by KIT. The mass of released hydrogen was found to be approximately eight times lower than the corresponding weight gain. While the weight gain of AISI 348 is relatively high compared to other ATF concepts, this also leads to higher hydrogen generation.

4. DISCUSSION

The weight gain after autoclave exposure was very low, between 1 and 2 mg dm^{-2}, which is close to the resolution limit of the balance. This proximity to the measurement accuracy likely contributed to the

scatter observed in the data. The sudden increase in WG recorded during the test may also be attributed to an impurity attached to the specimen or another experimental artifact.

Mössbauer spectroscopy primarily identified $FeCr_2O_3$ in the oxide layer after 63 days of exposure, with only weak indications of Fe-based oxides. After 1659 days in the simulated WWER environment, mixed iron oxides were confirmed. These results suggest either a slow evolution of the oxide composition or a limitation of the detection method, as Mössbauer spectroscopy can indicate but not unambiguously confirm the presence of iron oxides.

In contrast, XRD analysis reported by INCT in [1] detected Fe_2O_3 after only 42 days of autoclave exposure. The discrepancy may therefore arise from methodological differences between the two techniques as well as from variations in testing conditions.

For the high-temperature oxidation study, all available specimens were used in the experiments. As a result, no specimens remained for characterization in the as-received state. Consequently, measurements such as ring compression test (RCT), hydrogen content, and initial grain size were not performed prior to exposure. Although mechanical properties were provided with the specimens, they are not directly comparable due to differences in specimen geometry (standard tensile test vs. ring compression test). According to the supplier, the average grain size in the as-received condition was G 8–9. However, after exposure at 1 100 °C, a finer grain size of G 10.5 was observed. Since grain size reduction is not typically expected after annealing at 1 100 °C, it is likely that the actual initial grain size was closer to G 10.5.

One of the key challenges in employing AISI 348 stainless steel as a cladding material is the significant hydrogen generation under accident conditions. During normal operation, the measured weight gain remains relatively low. However, high-temperature oxidation tests revealed a marked increase in weight gain at elevated temperatures. If the oxidation process proceeds only through the reaction with water, oxygen from water decomposition contributes to oxide layer growth. The corresponding hydrogen is either absorbed by the material or released into the surrounding environment. Direct measurements showed only a small amount of hydrogen absorbed in the material. It can therefore be concluded that most of the hydrogen formed during high-temperature exposure was released into the environment.

The estimated hydrogen release relative to WG is presented in Table 4. The absorbed fraction was subtracted from the total hydrogen release, which was calculated using the molar masses of oxygen and hydrogen.

For comparison, PVD Cr-coated Zircaloy-2 plate specimens tested under the same conditions [1] exhibited a weight gain of around 8 $g\,m^{-2}$ at 1 100 °C and 12-13 $g\,m^{-2}$ at 1 200 and 1 300 °C, and correspondingly much lower hydrogen release than AISI 348.

Exposure [**°C/min**]	**WG** [$g\,m^{-2}$]	**Released hydrogen** [$g\,m^{-2}$]
1 100/60	73.7	9.2
1 200/30	61.9	7.7
1 300/5	112.2	14.0
1 400/2	217.4	27.1

Table 4. Estimated hydrogen released to the environment during high-temperature oxidation tests.

5. Conclusions

Long-term corrosion and high-temperature oxidation experiments were performed on stabilized stainless steel AISI 348.

Under simulated WWER primary circuit conditions, AISI 348 showed stable oxide formation and limited corrosion progression. This confirms its suitability for standard operational use.

At elevated temperatures, oxidation accelerated and caused significant hydrogen release into the environment. Despite this, the mechanical integrity of the material was largely preserved. Ductility after high-temperature oxidation remained high, and microhardness (HVM 0.1) values stayed close to the initial state. Microstructural changes were, however, evident: grain coarsening occurred after high-temperature exposure, and intergranular corrosion appeared after oxidation at 1 400 °C.

These findings suggest that while AISI 348 is suitable for standard operational use, its behaviour under accident scenarios requires further investigation, particularly with respect to hydrogen management and cladding integrity.

Acknowledgements

This work was supported by the project Center of Advanced Nuclear Technology II (TN02000012) funded by the Technology Agency of the Czech Republic; by the IAEA Coordinated Research Project T12032; and by the Large Research Infrastructures of the Ministry of Education, Youth and Sports of the Czech Republic (LM2023073).

References

[1] International Atomic Energy Agency. *Analysis of options and experimental examination of fuels for water cooled reactors with increased accident tolerance (ACTOF) (IAEA TECDOC No. 1921)*. International Atomic Energy Agency, 2020. ISBN 978-92-0-114220-7.

[2] R. E. Pawel, J. V. Cathcart, R. A. McKee. The kinetics of oxidation of Zircaloy-4 in steam at high temperatures. *Journal of The Electrochemical Society* **126**(7):1105–1111, 1979. https://doi.org/10.1149/1.2129227

[3] M. Ševeček, A. Gurgen, A. Seshadri, et al. Development of Cr cold spray-coated fuel cladding with enhanced accident tolerance. *Nuclear Engineering and Technology* **50**(2):229–236, 2018. Special issue on the

water reactor fuel performance meeting 2017 (WRFPM 2017). https://doi.org/10.1016/j.net.2017.12.011

[4] T. Žák, Y. Jirásková. CONFIT: Mössbauer spectra fitting program. *Surface and Interface Analysis* **38**(4):710–714, 2006. https://doi.org/10.1002/sia.2285

[5] F. B. Waanders, S. W. Vorster, A. Engelbrecht. Mössbauer and SEM characterisation of the scale on type 304 stainless steel. *Scripta Materialia* **42**(10):997–1000, 2000. https://doi.org/10.1016/S1359-6462(00)00322-5

[6] A. G. B. Dominguez, M. I. Valerio-Cuadros, L. E. Borja-Castro, et al. Characterization and Mössbauer spectroscopy of steel slag generated in the ladle furnance in SIDERPERU steel plant. *Hyperfine Interactions* **243**:12, 2022. https://doi.org/10.1007/s10751-022-01799-x

[7] M. D. Osborne, M. E. Fleet, G. Michael Bancroft. Fe^{2+} -Fe^{3+} ordering in chromite and Cr-bearing spinels. *Contributions to Mineralogy and Petrology* **77**:251–255, 1981. https://doi.org/10.1007/BF00373539

[8] ČSN EN ISO 643, Ocel – Mikrografické stanovení zdánlivé velikosti zrn [In Czech; Steels – Micrographic determination of the apparent grain size], 2024.

[9] ČSN EN ISO 6507-1:2024 (420374) – Kovové materiály – Zkouška tvrdosti podle Vickerse – Část 1: Zkušební metoda [In Czech; Metallic materials – Vickers hardness test – Part 1: Test method], 2024.